
**STRENGTH
AND PLASTICITY**

Evolution of the Structure, Texture, and Mechanical Properties of Austenitic Stainless Steel during Annealing after Cold Radial Forging

**R. S. Chernichenko^{a, *}, D. O. Panov^{a, **}, S. V. Naumov^a, E. A. Kudryavtsev^a,
V. V. Mirontsov^a, G. A. Salishchev^a, and A. S. Pertsev^b**

^a *Belgorod State University, Belgorod, 308015 Russia*

^b *Perm Scientific Research Technological Institute, Perm, 614600 Russia*

^{*}*e-mail: chernichenko@bsu.edu.ru*

^{**}*e-mail: dimmak-panov@mail.ru*

Received January 27, 2023; revised April 4, 2023; accepted April 7, 2023

Abstract—The effect of annealing temperature on the structure, texture, and mechanical properties of the austenitic 08Kh16N13M2T stainless steel after cold radial forging to a degree of 95% has been investigated. Preliminary plastic deformation results in the formation of austenitic structural and $\langle 111 \rangle$ and $\langle 100 \rangle$ textural gradients. Low-temperature annealing (500–600°C) causes structural polygonization. The intensity of the $\langle 111 \rangle$ and $\langle 100 \rangle$ textural components remains unchanged. Annealing at 700°C initiates recrystallization only in the surface layers of the bar. Annealing at 800–900°C results in static recrystallization processes throughout the bar cross section, which blurs the textural gradient. Annealing at 400–600°C increases the strength and hardness properties. Moreover, the plasticity increases with increasing annealing temperature. Annealing at 700°C makes the material soften almost to the level of the initial cold-deformed state and significantly increases its plasticity.

Keywords: austenitic steel, structure, texture, radial forging, strength, plasticity

DOI: 10.1134/S0031918X23600537

INTRODUCTION

Austenitic stainless steels, due to their excellent oxidation resistance, high ductility, and high impact toughness at room and low temperatures, are used in the marine, aerospace, automotive, petrochemical, and nuclear industries, as well as in medicine [1–6]. However, this steel has a very significant disadvantage, which is its low yield strength.

Many studies have been carried out to improve the yield strength of austenitic steels [7–14]. For example, room-temperature rolling (to $\epsilon = 75\%$) of austenitic stainless steel 17Cr–14Ni–3Mo significantly increases its yield strength because of austenite structure fragmentation, but such a treatment decreases the plasticity of this steel [13]. On the other hand, strength can be increased without decreasing plasticity via the formation of heterogeneous structures consisting of differently sized structural elements [7, 8]. For example, dynamic forging and subsequent annealing in the temperature range 730–800°C resulted in the formation of a heterogeneous structure consisting of nonrecrystallized twinned regions and large defect-free recrystallized grains, which provided the synergy of the strength and plasticity of 316L stainless austenitic steel [7]. An alternative way to achieve high strength and

plastic properties consists in creating homogeneous nanocrystalline (NC) and ultrafine grained (UFG) structures with low dislocation number density. For example, austenitic 316 stainless steel is reported to have excellent mechanical properties after high-pressure torsion, which results in an UFG structure, and subsequent short-term annealing aimed at reducing dislocation density [8]. However, it is quite difficult to produce a billet for industrial applications by the techniques used in [7, 8].

Commercial billets with high yield strength can be produced by cold radial forging (CRF) [9–12]. CRF deformation of austenitic steels [10, 11] increased dislocation density and a number of deformation twins and resulted in structure fragmentation, which increased the yield strength of 08Kh16N13M2T steel by more than four times (from 243 to 1076 MPa) and significantly reduced its relative elongation (from 62 to 9%). Therefore, CRF is a promising commercial technique for improving yield strength, but more research is needed to determine the conditions for achieving good plasticity without loss of strength. However, we know that the optimum combination of strength and plasticity can be achieved by cold plastic deformation and subsequent annealing [7, 9]. This work is aimed at

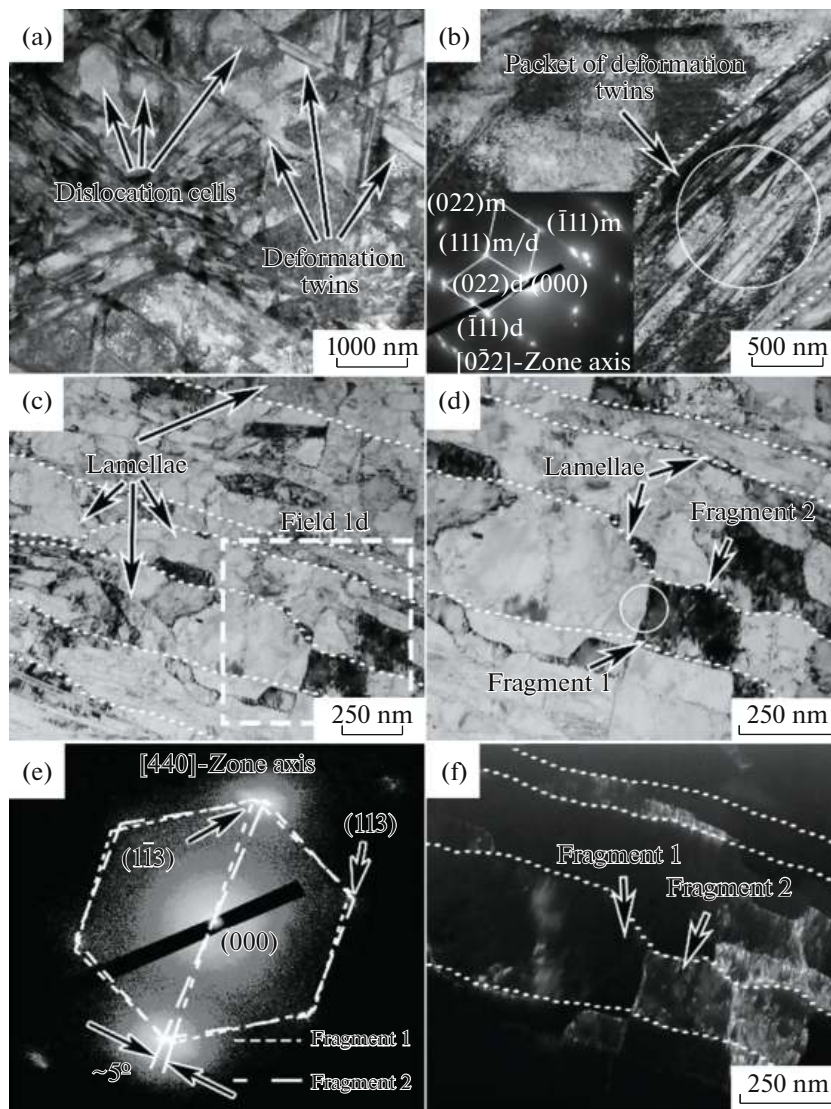


Fig. 1. The results of TEM investigation of (a, b) the center and (c–f) surface layer of the bar: (a–d) bright-field images; (e) electron diffraction pattern taken from the region of the microstructure indicated by a white circle at Fig. 1d; (f) dark-field image taken in the austenitic reflection (113) of fragment 2 (Fr. 2). (b) The electron diffraction pattern taken from the microstructure region indicated by the white circle at Fig. 1d.

investigating the evolution of the structure, texture, and mechanical properties of austenitic CRF-treated stainless steel during postdeformation annealing.

EXPERIMENTAL

The material under study was 08Kh16N13M2T steel of the following chemical composition: 0.08% C, 16.4% Cr, 12.3% Ni, 2.18% Mo, 1.28% Mn, 0.42% Si, 0.2% Ti, and Fe for balance. A steel ingot was preliminarily subjected to hot radial forging to $\varnothing 46$ mm and then quenched at 1050°C in air. The resulting bar was then deformed by the CRF technique by five passes: 20% (from 46 to 35 mm), 40% (from 35 to 30 mm), 60% (from 30 to 25 mm), 80% (from 25 to 17 mm), and 95% (from 17 to 12.6 mm) of the initial cross sec-

tional area of the bar. The state after 95% deformation was taken as the initial state for the subsequent annealing. The resulting bar was annealed at temperatures of 400, 500, 550, 600, 700, 800, and 900°C for 2 h and cooled in air.

Transmission electron microscopy (TEM) studies were performed on thin foils using a JEOL JEM-2100 transmission electron microscope at an accelerating voltage of 200 kV. Standard techniques were used to prepare the foils [10]. Scanning electron microscopy (SEM) studies were performed on the surface of thin foils using a FEI Nova NanoSEM 450 scanning electron microscope equipped with an EDAX Hikari EBSD camera. The scanning step was 200 nm to build crystallographic misorientation maps. Vickers hard-

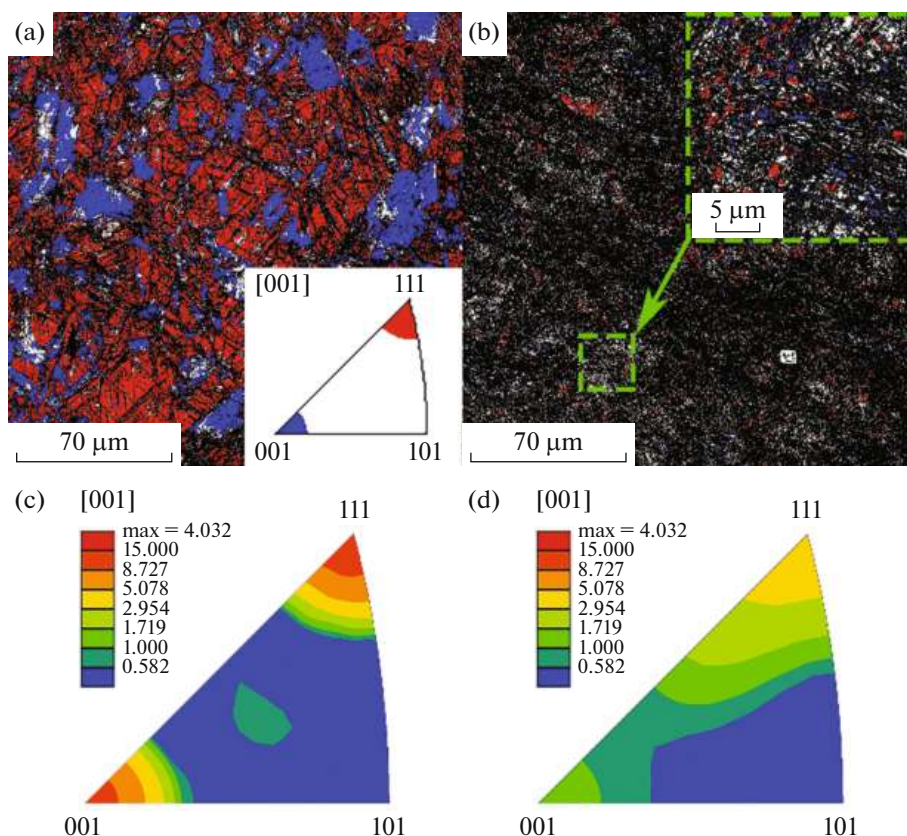


Fig. 2. (a), (b) Orientation distribution maps and (c), (d) inverse pole figures for the initial deformed state in the (a), (c) center and (b), (d) surface layer of the bar.

ness was determined on a Wolpert 402MVD microhardness tester equipped with a diamond pyramid with an apex angle of 136° . The load applied was 200 g, and the holding time was 15 s. The measurements were made in the cross section along two mutually perpendicular diameters and the results were averaged. Uniaxial tensile tests were performed at room temperature and strain rate of $1.2 \times 10^{-3} \text{ s}^{-1}$ using an Instron 5882 universal tester. Flat test specimens were cut from the central part of the bar along the axis. All structural zones of the material were observed in the cross section of these specimens. The sizes of the specimens were calculated according to GOST 1497–84.

Steel structure in the initial cold-deformed state.

After CRF to a degree of 95%, the steel exhibits mainly austenitic structure [10]. The structural and textural gradients were detected along the cross section of the bar. Electron microscopy studies of the cross section of the bar showed that the structure in the central part was fragmented by single deformation twins of different systems and dislocation cells (Fig. 1a), as well as by twin packets (Fig. 1b). The surface layers had mainly lamellar structure (Fig. 1c). Microdiffraction and dark-field analysis (Figs. 1e, 1f) show that a fragmented submicrocrystalline structure with low-angle misorientations of less than 15° formed along lamellas. Cold plastic deformation with high degrees resulted in the for-

mation of submicrograins with an average diameter of 100–200 nm and a low defect density in them [15, 16]. Similar single structural elements were also found previously in the surface layers of severely deformed samples of the material under study [10].

RESULTS AND DISCUSSION

Cold radial forging also results in the formation of a sharp axial texture $\langle 001 \rangle \parallel$ bar axis (BA) and $\langle 111 \rangle \parallel$ BA in the center of the bar (Figs. 2a, 2c), which is smeared towards the edge (Figs. 2b, 2d). The volume fraction of crystals with $\langle 001 \rangle \parallel$ BA orientation decreases from 37 to 6–16% with distance from the center to the edge, respectively. The volume fraction of crystals with $\langle 111 \rangle \parallel$ BA orientation in the center of the bar and at half of the radius is about the same level (50–60%). However, the volume fraction of these crystals also decreases to 18% as we move toward the edge. The development of the $\langle 111 \rangle \parallel$ BA component during CRF is due to the twinning of the austenite grains [10, 17], whereas the grains with the $\langle 001 \rangle \parallel$ BA orientation are textured due to dislocation slip. The formation of the initial state was described in detail in [10].

Evolution of fine structure during postdeformation annealing. Figure 3 shows the results of the study of the fine 08Kh16N13M2T steel structure after annealing.

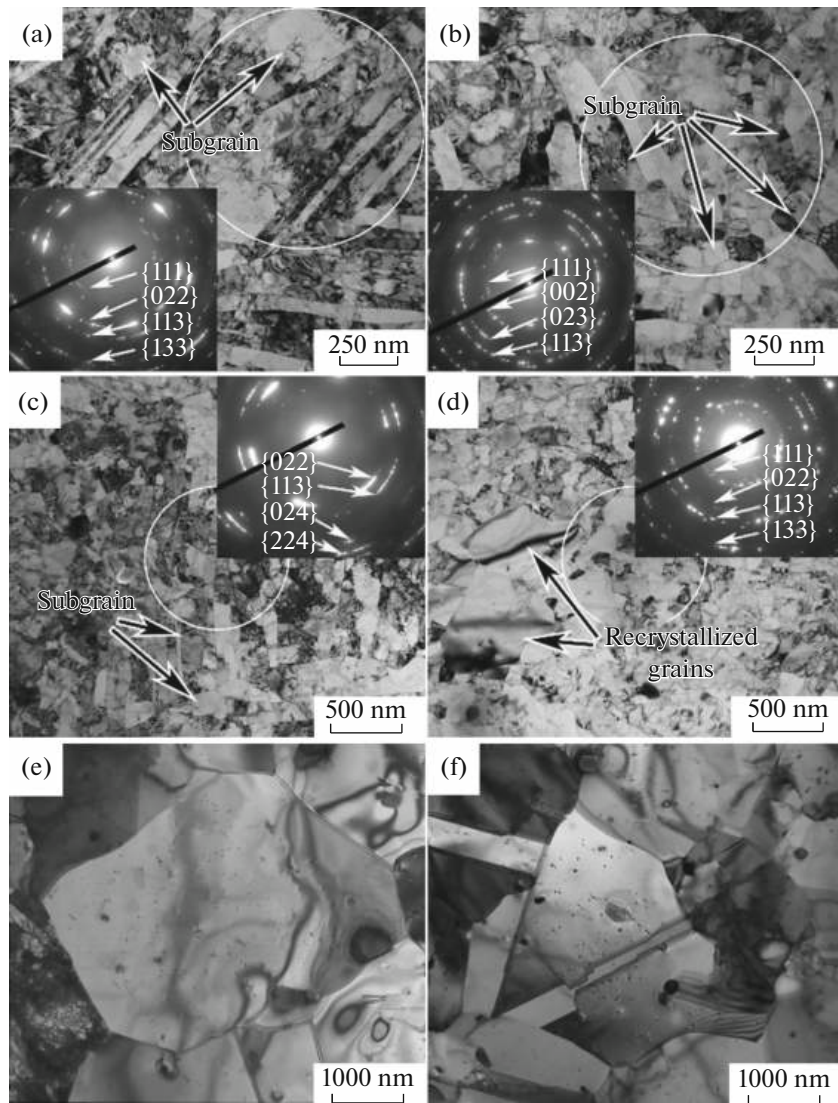


Fig. 3. TEM study of the (a, c, e) center and (b, d, f) surface of the bar annealed at different temperatures: (a, b) 600, (c, d) 700, and (e, f) 800°C. (a–c) The electron diffraction pattern taken from the microstructure region indicated by the white circle.

Postdeformation annealing at 500–600°C resulted in similar structural changes. For example, dislocation-free subgrains form and mechanical twins/lamellae are fragmented in the central part (Fig. 3a) and in the surface layers (Fig. 3b) of the bar. These processes develop more actively in the surface layer. As well, the formation of the subgrain structure with a subgrain size of about 100 nm is more pronounced in the surface layer (Fig. 3b). An increase in the annealing temperature to 700°C provides a further redistribution of dislocations in the center of the bar (Fig. 3c) and the formation of a subgrain structure. Meanwhile, new large defect-free grains about 500 nm in size were observed in the surface layer (Fig. 3d), which apparently resulted from the development of static recrystallization [14].

A further increase in the annealing temperature to 800°C causes a complete recrystallization of the cold-

deformed structure and the formation of equiaxed defect-free austenite grains 4–6 μm in size both in the central part of the bar and in the surface layer (Figs. 3e, 3f). As a result, the structural gradient formed during the preliminary CRF disappears.

Texture evolution during postdeformation annealing.

The orientation distribution maps and inverse pole figures of the investigated steel after annealing are shown in Fig. 4. After annealing at 600–700°C, a sharp $\langle 001 \rangle \parallel \text{BA}$ and $\langle 111 \rangle \parallel \text{BA}$ texture are observed in the center of the bar. As the annealing temperature increases to 800–900°C, the sharpness of both the $\langle 001 \rangle \parallel \text{BA}$ and $\langle 111 \rangle \parallel \text{BA}$ components decreases. The smeared axial $\langle 001 \rangle \parallel \text{BA}$ and $\langle 111 \rangle \parallel \text{BA}$ texture components are observed in the surface layer of the bar in all cases. The annealing temperature has a weak effect on the characteristics of this texture.

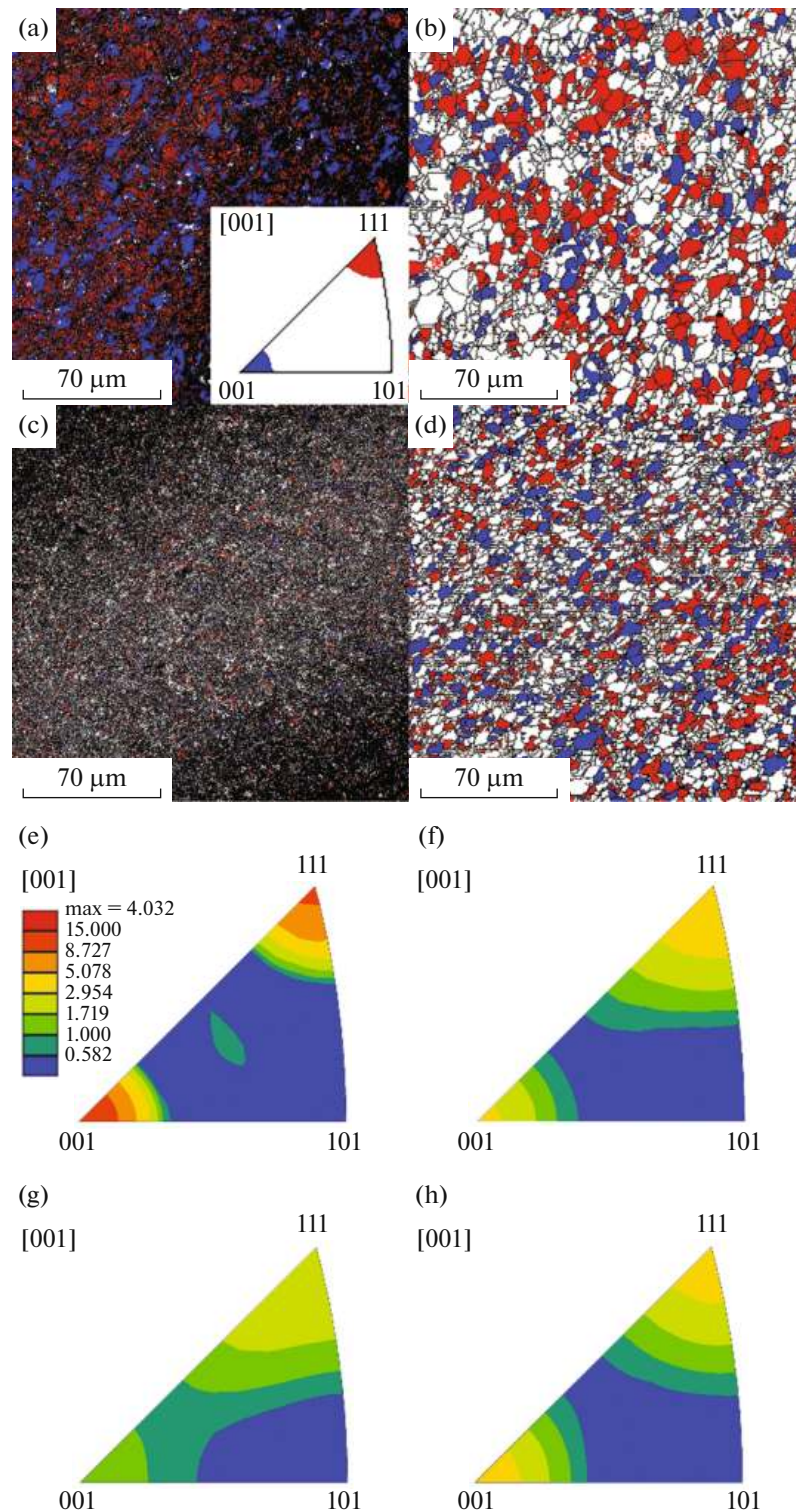


Fig. 4. (a–d) Orientation distribution maps and (e–h) inverse pole figures for the (a, b, e, f) center and (c, d, g, h) surface layer of the bar annealed at different temperatures: (a, c, e, g) 600 and (b, d, f, h) 900°C.

In addition, the fraction of grains with orientations $\langle 111 \rangle \parallel \text{BA}$ and $\langle 001 \rangle \parallel \text{BA}$ as a function of annealing temperature was built (Fig. 5). After annealing at 600 and 700°C the fraction of $\langle 111 \rangle \parallel \text{BA}$ oriented grains remains 50–60% in the central part and at half of the

bar radius (Fig. 5a). The fraction of grains with this orientation does not exceed 16–17% in the surface layer. Annealing at higher temperatures (800–900°C) results in the levelling of the fraction of $\langle 111 \rangle \parallel \text{BA}$ oriented grains over the bar cross section at the level of

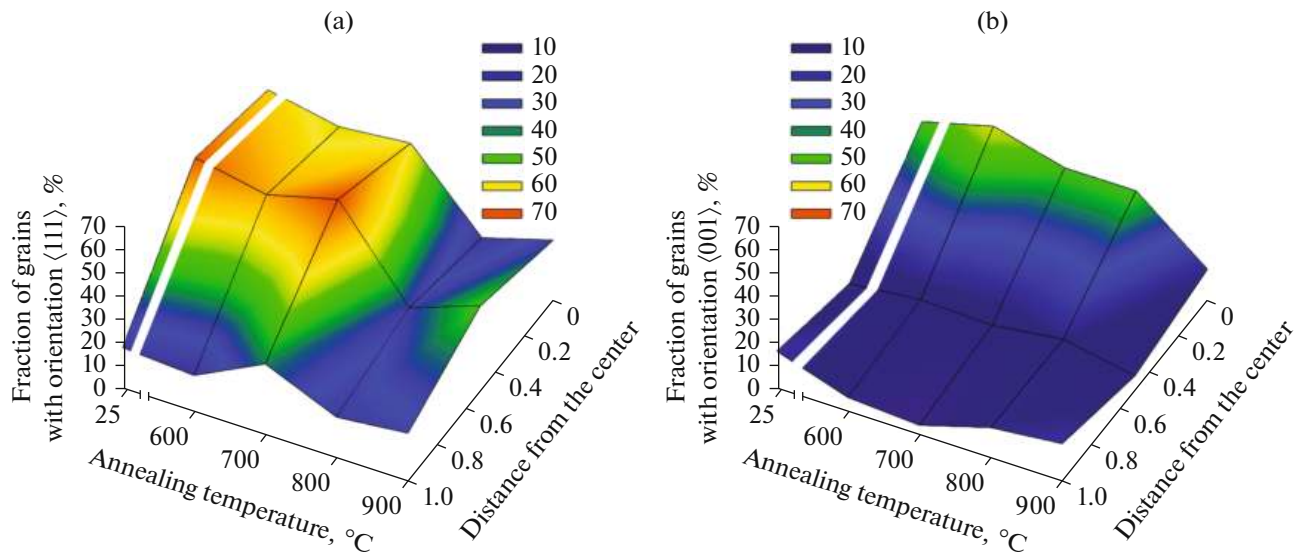


Fig. 5. Annealing temperature effect on the distribution of the volume fraction of grains with textural (a) $\langle 111 \rangle ||$ (BA) and (b) $\langle 001 \rangle ||$ (BA) components.

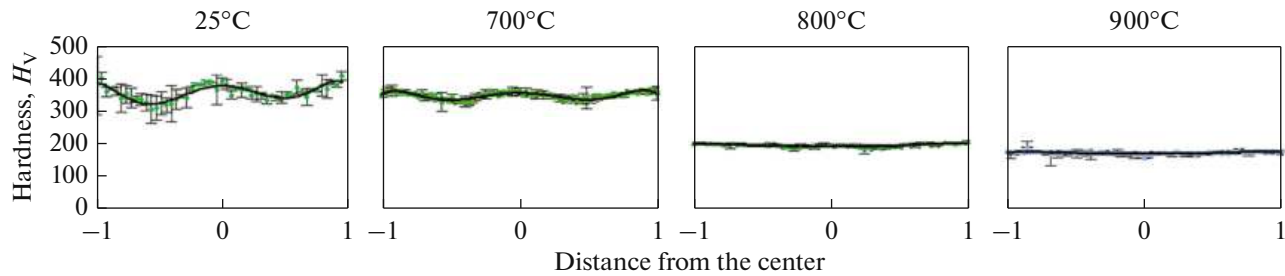


Fig. 6. The hardness distribution across the bar cross section after 95% CRF and annealing at different temperatures.

17–25%. On the other hand, for each annealing temperature, the maximum volume fraction of $\langle 001 \rangle ||$ BA oriented crystals is observed in the center of the bar (Fig. 5b). The initial gradient of the textural $\langle 001 \rangle ||$ BA component is retained along the direction from the center to the edge of the bar after annealing at 600–800°C. The fraction of crystals with the $\langle 001 \rangle ||$ (BA) orientation leveled (to 11%) throughout the cross section of the bar, when the annealing temperature is increased to 900°C.

Finally, annealing at 600–700°C retains the initial twinned structure in the center of the bar, so that the volume fraction of grains with the $\langle 111 \rangle ||$ (BA) orientation does not change. We should note that the volume fraction of $\langle 001 \rangle ||$ (BA) oriented grains decreases slightly in this case, apparently due to the redistribution of dislocations during polygonization. Static recrystallization processes tend to decrease the volume fraction of $\langle 111 \rangle ||$ (BA) and $\langle 001 \rangle ||$ (BA) oriented grains when the annealing temperature increases to 800 and 900°C, respectively. The lower thermal stability of

$\langle 111 \rangle ||$ (BA) oriented grains is caused by the accumulation of a large number of defects during CRF due to the simultaneous development of mechanical twinning and dislocation slip, as compared to $\langle 001 \rangle ||$ (BA) grains where dislocation slip predominated.

The annealing effect on the hardness distribution over the cross section of the bar. Hardness measurements showed that hardness in the initial state is not uniformly distributed across the cross section of the bar and ranges from 350 to 400 H_V (Fig. 6). The maximum hardness is in the surface layer of the bar. It decreases to a minimum at half the radius and reaches its maximum in the central part. Annealing at temperatures of 400–600°C does not change the value and pattern of cross sectional hardness distribution significantly. However, annealing at 700°C slightly reduces the hardness of the steel under study and makes it more homogeneous along the cross section (Fig. 6). The hardness values range from 315 to 355 H_V . Annealing at 800–900°C decreases the hardness and

aligns it to the level of 165–170 H_V across the section of the bar.

The nonuniform distribution of hardness over the bar cross section can probably be explained by the presence of residual stresses generated by CRF [18, 19]. The compressive and tensile stresses were generated in the center and surface layers, respectively, whereas compressive stresses fully compensate tensile stresses at half the radius, causing a minimum of hardness there. Residual stresses are obviously retained up to 700°C, and an increase in the annealing temperature up to 800°C removes them and equalizes the hardness across the section.

The annealing effect on mechanical properties. In the initial state, a tensile diagram (Fig. 7a) is typical of cold-deformed austenitic steel with high strength ($\sigma_u = 1217$ MPa, $\sigma_{0.2} = 1077$ MPa) and low plasticity ($\delta = 9.4\%$) (Fig. 7b). The uniform strain is 1.7% and the localized strain is 7.7%. Annealing at 400°C does not change the tensile diagram, but the yield strength ($\sigma_{0.2}$) increases considerably to 1381 MPa and the tensile strength (σ_u) to 1402 MPa. The relative elongation (δ) decreases to 7.4%, and the uniform elongation δ_{uni} decreases to 0.6%. After annealing at 500–600°C, $\sigma_{0.2}$ and σ_u stabilize at 1310–1350 and 1360–1380 MPa, respectively (Fig. 7b). The plasticity properties increase (δ grows to 10.5%), but δ_{uni} remains at the level of 0.6–0.7%. However, annealing at 700°C changes the tensile diagram, namely, an extended strain-hardening region of ~8.5% appears. The strength properties decrease virtually to the level of the initial cold-deformed state ($\sigma_{0.2}$ to 1027 MPa, σ_u to 1145 MPa) and the plasticity increases (δ to 16.1%).

On the one hand, the increase and subsequent stabilization of the strength after annealing in the temperature range 400–600°C are probably the result of the formation of segregation of the alloying elements at dislocations. As is shown in [20], the formation of grain boundary Mo–Cr–Si segregations in these steels increases the critical stress threshold necessary for a boundary to have dislocations; as a result, the yield strength of the material increases. In addition, such segregations pin dislocations, which also increases threshold stresses and, as a result, increases strength. On the other hand, the plasticity of steel increases when the annealing temperature is increased from 400 to 600°C due to the redistribution of dislocations throughout the volume of the material and dislocation-free microvolumes are expected to form; therefore, the material can be plastically deformed due to dislocation movement along the dislocation-free microvolumes. A gradient structure, where surface layers are initially more hardened than the core, also contributes to a good combination of strength and plasticity due to the redistribution of strains and stresses between the center and the more hardened

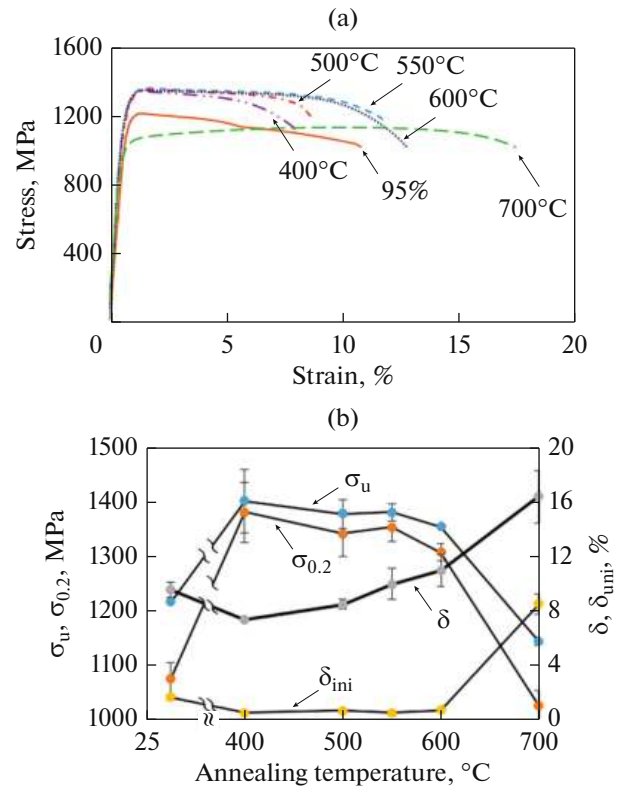


Fig. 7. (a) The stress–strain curves and (b) tensile properties of the steel.

edge of a bar [10]. An increase in the annealing temperature to 700°C causes a decrease in strength owing to the development of static recrystallization in the surface layers [14], which is also accompanied by an increase in plasticity due to the formation of defect-free austenitic grains (Fig. 3d).

CONCLUSIONS

The effect of the annealing temperature on the evolution of the structure, texture, and mechanical properties of the initially cold-deformed 08Kh16N13M2T austenitic stainless steel was investigated. The following conclusions were drawn from the study:

(1) Annealing at 400–600°C cleans subgrains from dislocations and causes the fragmentation of mechanical twins. A subgrain structure forms in the surface layer. Annealing at 700°C results in the formation and growth of recrystallization nuclei in the surface layer and the formation of a subgrain structure in the center of the bar. Annealing at 800–900°C causes complete recrystallization of the initial deformed structure.

(2) Cold radial forging forms a gradient of two-component axial texture in the bar ($\langle 001 \rangle$, $\langle 111 \rangle$), with the intensity of the texture decreasing from the center to the edge of the bar. Annealing in the temperature range 600–700°C slightly reduces the $\langle 001 \rangle$ texture

intensity in the center of the bar and keeps the $\langle 111 \rangle$ texture intensity at the same level. An increase in the annealing temperature to 800 and 900°C smears the gradients of $\langle 111 \rangle$ and $\langle 001 \rangle$ textures, respectively.

(3) After 95% CRF, the hardness is nonuniformly distributed across the cross section of the bar. The hardness level and its distribution pattern across the cross section remain the same after annealing at 400–600°C. An increase in the annealing temperature to 700°C reduces the hardness. Annealing at temperatures of 800–900°C levels out and decreases the general hardness across the cross section of the bar.

(4) Annealing at temperatures of 400–600°C increases the strength of initially cold-deformed steel ($\sigma_{0.2}$ to ~1350 MPa, σ_u to 1380 MPa). The relative elongation gradually increases (from 7.4 to 10.5%) as the annealing temperature increases. A further increase in the annealing temperature to 700°C increases the plasticity (δ to 16.1%) and decreases the strength characteristics almost to the level of the initial cold-deformed state ($\sigma_{0.2}$ to 1027 MPa, σ_u to 1145 MPa).

ACKNOWLEDGMENTS

The study was performed at the Technologies and Materials Center of the Collaborative Access, Belgorod State University.

FUNDING

This work was supported by the Russian Scientific Foundation (project no. 20-79-10094).

CONFLICT OF INTEREST

The authors of this work declare that they have no conflicts of interest.

REFERENCES

1. S. Chattopadhyay, G. Anand, S. G. Chowdhury, and I. Manna, “Effect of reverse austenitic transformation on mechanical property and associated texture evolution in AISI 316 austenitic stainless steel processed by low temperature rolling and annealing,” *Mater. Sci. Eng., A* **734**, 139–148 (2018).
<https://doi.org/10.1016/j.msea.2018.07.087>
2. J. S. Lu, Q. S. Lu, and J. Xue, “Corrosion resistance of three 316 stainless steels,” *Adv. Mater. Res.* **936**, 1097–1101 (2014).
[doi 10.4028/www.scientific.net/amr.936.1097](https://doi.org/10.4028/www.scientific.net/amr.936.1097)
3. D. Panov, A. Pertsev, A. Smirnov, V. Khotinov, and Yu. Simonov, “Metastable austenitic steel structure and mechanical properties evolution in the process of cold radial forging,” *Materials* **12**, 2058 (2019).
<https://doi.org/10.3390/ma12132058>
4. A. Saboori, A. Aversa, G. Marchese, S. Biamino, M. Lombardi, and P. Fino, “Microstructure and mechanical properties of AISI 316L produced by directed energy deposition-based additive manufacturing: A review,” *Appl. Sci.* **10**, 3310 (2020).
<https://doi.org/10.3390/app10093310>
5. Q. Wang, M. Zhang, C. Yang, Yi. Yang, E. Zhou, P. Liu, D. Jin, D. Xu, L. Wu, and F. Wang, “Oral microbiota accelerates corrosion of 316L stainless steel for orthodontic applications,” *J. Mater. Sci. Technol.* **128**, 118–132 (2022).
<https://doi.org/10.1016/j.jmst.2022.04.012>
6. G. T. Gray, V. Livescu, P. A. Rigg, C. P. Trujillo, C. M. Cady, S. R. Chen, J. S. Carpenter, T. J. Lienert, and S. J. Fensin, “Structure/property (constitutive and spallation response) of additively manufactured 316L stainless steel,” *Acta Mater.* **138**, 140–149 (2017).
<https://doi.org/10.1016/j.actamat.2017.07.045>
7. F. K. Yan, G. Z. Liu, N. R. Tao, and K. Lu, “Strength and ductility of 316L austenitic stainless steel strengthened by nano-scale twin bundles,” *Acta Mater.* **60**, 1059–1071 (2012).
<https://doi.org/10.1016/j.actamat.2011.11.009>
8. M. Liu, W. Gong, R. Zheng, J. Li, Z. Zhang, S. Gao, C. Ma, and N. Tsuji, “Achieving excellent mechanical properties in type 316 stainless steel by tailoring grain size in homogeneously recovered or recrystallized nanostructures,” *Acta Mater.* **226**, 117629 (2022).
<https://doi.org/10.1016/j.actamat.2022.117629>
9. Yu. Wu, X. Dong, and Q. Yu, “An upper bound solution of axial metal flow in cold radial forging process of rods,” *Int. J. Mech. Sci.* **85**, 120–129 (2014).
<https://doi.org/10.1016/j.ijmecsci.2014.05.019>
10. D. Panov, R. Chernichenko, E. Kudryavtsev, D. Klimenko, S. Naumov, and A. Pertcev, “Effect of cold swaging on the bulk gradient structure formation and mechanical properties of a 316-type austenitic stainless steel,” *Materials* **15** (7), 2468 (2022).
<https://doi.org/10.3390/ma15072468>
11. D. O. Panov, R. S. Chernichenko, S. V. Naumov, A. S. Pertcev, N. D. Stepanov, S. V. Zherebtsov, and G. A. Salishchev, “Excellent strength-toughness synergy in metastable austenitic stainless steel due to gradient structure formation,” *Mater. Lett.* **303**, 130585 (2021).
<https://doi.org/10.1016/j.matlet.2021.130585>
12. D. O. Panov, A. I. Smirnov, and A. S. Pertsev, “Formation of structure in metastable austenitic steel during cold plastic deformation by the radial forging method,” *Phys. Met. Metallogr.* **120**, 184–190 (2019).
<https://doi.org/10.1134/s0031918x19020145>
13. S. A. Akkuzin and I. Yu. Litovchenko, “The influence of deformation and short-term hightemperature annealing on the microstructure and mechanical properties of austenitic steel 17Cr–14Ni–3Mo (316 type),” *Russ. Phys. J.* **62**, 1511–1517 (2019).
<https://doi.org/10.1007/s11182-019-01870-1>
14. M. M. Abramova, N. A. Enikeev, R. Z. Valiev, X. Sauvage, A. Etienne, B. Radiguet, and E. Ubyivovk, “Thermal stability and extra-strength of an ultrafine grained stainless steel produced by high pressure torsion,” *Rev. Adv. Mater. Sci.* **43**, 83–88 (2015).

15. N. A. Smirnova, V. I. Levit, V. I. Pilyugin, R. I. Kuznetsov, L. S. Davydova, and V. A. Sazonova, "Evolution of structure of fcc single crystals during strong plastic deformation," *Phys. Met. Metallogr.* **61** (6), 127–134 (1986).
16. A. M. Glezer, A. A. Tomchuk, and A. O. Cheretaeva, "Structure and mechanical properties of carbon steel, processed in Bridgeman camera by torsion deformation in different directions," *Vestn. Tomsk. Gos. Univ.* **18** (4-2), 1946–1947 (2013) [in Russian].
17. I. Karaman, H. Sehitoglu, Y. I. Chumlyakov, and H. J. Maier, "The deformation of low-stacking-fault-energy austenitic steels," *JOM* **54** (7), 31–37 (2002). <https://doi.org/10.1007/bf02700983>
18. G. Singh, B. Kalita, K. I. Vishnu Narayanan, U. K. Aroora, M. M. Mahapatra, and R. Jayaganthan, "Finite element analysis and experimental evaluation of residual stress of Zr-4 alloys processed through swaging," *Metals* **10**, 1281 (2020). <https://doi.org/10.3390/met10101281>
19. D. Panov, E. Kudryavtsev, S. Naumov, D. Klimenko, R. Chernichenko, V. Mirontsov, N. Stepanov, S. Zhe-rebtsov, G. Salishchev, and A. Pertcev, "Gradient microstructure and texture formation in a metastable austenitic stainless steel during cold rotary swaging," *Materials* **16**, 1706 (2023). <https://doi.org/10.3390/ma16041706>
20. M. M. Abramova, N. A. Enikeev, R. Z. Valiev, A. Etienne, B. Radiguet, Y. Ivanisenko, and X. Sauvage, "Grain boundary segregation induced strengthening of an ultrafine-grained austenitic stainless steel," *Mater. Lett.* **136**, 349–352 (2014). <https://doi.org/10.1016/j.matlet.2014.07.188>

Translated by T. Gapontseva